

Experimental assessment of the Refined Zigzag Theory for the static bending analysis of sandwich beams

Original

Experimental assessment of the Refined Zigzag Theory for the static bending analysis of sandwich beams / Iurlaro, Luigi; Gherlone, Marco; Mattone, Massimiliano Corrado; Di Sciuva, Marco. - In: JOURNAL OF SANDWICH STRUCTURES AND MATERIALS. - ISSN 1099-6362. - ELETTRONICO. - 20:1(2018), pp. 86-105.
[10.1177/1099636216650614]

Availability:

This version is available at: 11583/2689628 since: 2019-07-09T16:24:33Z

Publisher:

SAGE PUBLICATIONS LTD Lancaster, PA

Published

DOI:10.1177/1099636216650614

Terms of use:

This article is made available under terms and conditions as specified in the corresponding bibliographic description in the repository

Publisher copyright

(Article begins on next page)

Experimental assessment of the Refined Zigzag Theory for the static bending analysis of sandwich beams

Luigi Iurlaro, Marco Gherlone, Massimiliano Mattone, Marco Di Sciuva

Abstract In the present work, for the first time, the accuracy of the Refined Zigzag Theory (RZT) in reproducing the static bending response of sandwich beams is experimentally assessed. The theory is briefly reviewed and an analytical solution of the equilibrium equations is presented for the boundary and loading conditions under investigation (four-point bending). The experimental campaign is described, including the material characterization and the bending tests. Experimentally measured deflections and axial strains are compared with those provided by RZT and by the Timoshenko Beam Theory with an ad-hoc shear correction factor. The Refined Zigzag Theory is

Politecnico di Torino, Department of Mechanical and Aerospace Engineering, Corso Duca degli Abruzzi 24, 1029 Torino (Italy)

Corresponding author:

M. Gherlone, Politecnico di Torino, Department of Mechanical and Aerospace Engineering, Corso Duca degli Abruzzi 24, 1029 Torino (Italy)

e-mail: marco.gherlone@polito.it

1
2
3
4
5
6
7
8
9 shown to be more accurate than the Timoshenko Beam Theory in particular for beams
10 with higher face-to-core thickness and stiffness ratios and with a reduced slenderness.
11
12

13
14
15 **Key Words** Sandwich beam, Rohacell[®], Refined Zigzag Theory, Four-point bending
16 test, Experimental assessment
17
18

19 20 21 22 **1 Introduction** 23

24
25
26
27 The consolidated application of multilayered composite and sandwich structures for
28 aircraft, naval, and automotive load-carrying components represents a challenge for
29 engineers and researchers. The mechanical behavior of laminated structures is, in fact,
30 strongly influenced by an inherent ply-wise heterogeneity and the through-the-thickness
31 distributions of displacements, strains and stresses can show complex patterns. This is
32 exacerbated in sandwich structures where the stiffness ratio between the external layers
33 (face-sheets) and the internal ply (core) is usually high. Moreover, the core of sandwich
34 constructions can exhibit three-dimensional geometries (honeycomb or corrugated) that
35 lead to even more complex structural responses [1].
36
37
38
39
40
41
42
43
44
45
46

47 High-fidelity, three-dimensional **Finite Element (FE)** models based on commercial
48 codes can provide accurate response predictions but at the cost of a large number of
49 degrees of freedom (especially if the core geometry is meshed in details) [1]. A
50
51
52
53
54
55
56
57
58
59
60

1
2
3
4
5
6
7
8
9 remarkable reduction in the computational complexity is achieved if the core is
10 substituted by a homogeneous and orthotropic equivalent material that can be then
11 included into the stacking sequence of the laminate [2]. Nevertheless, the key modeling
12 step is the selection of an efficient two-dimensional or one-dimensional theory for the
13 analysis of the sandwich structure. On one hand, the use of layer-wise theories (where
14 the distribution of the unknown displacements and/or stresses is assumed within each
15 layer) guarantees a satisfactory accuracy [3] but can be computationally too expensive
16 for complex analyses (non-linear, progressive failure) on laminated structures with
17 several layers. On the other hand, equivalent single layer theories (where the assumption
18 on the unknown variables is made over the whole laminate thickness) are based on a
19 reduced number of degrees of freedom but provide poor response predictions for thick
20 and/or highly heterogeneous laminated structures [4].
21
22
23
24
25
26
27
28
29
30
31
32
33
34

35 Due to their typical lay-up, with two external stiff faces and one internal weak core,
36 sandwich structures have been usually modeled with ad-hoc simplified approaches
37 based on reliable assumptions [5,6] and adopted in international standards for
38 experimental tests: faces carry in-plane loads and the core mainly carry transverse shear
39 deformation, therefore in-plane stresses are negligible in the core whereas transverse
40 shear stresses are negligible in the faces. These assumptions are valid in particular for
41 thin plates and slender beams and face-sheets much thinner than the core. Primary, load-
42 carrying sandwich components can be thick and with laminated face-sheets and the
43
44
45
46
47
48
49
50
51
52
53
54
55
56
57
58
59
60

1
2
3
4
5
6
7
8
9 classical assumptions lose their applicability. Higher-order theories have been proposed
10 to overcome this limitations, for example in [7] where Frostig et al. present the HSAPT,
11 High-order SAndwich Panel Theory. Both face-sheets are considered as Bernoulli-
12 Euler's beams whereas the core is modeled within the assumptions of plane stress and
13 including both transverse shear and normal deformability. The unknown variables of the
14 problem are the axial and transverse displacement of the face-sheets and the transverse
15 shear stress of the core layer. The approach is accurate in evaluating the local effects on
16 transverse stresses within the core due to the application of concentrated forces.

17
18
19
20
21
22
23
24
25
26 Within this context, interesting approaches are the so-called zigzag theories. They
27 represent an efficient compromise between accuracy and computational cost (the
28 number of kinematic variables is fixed, regardless the number of physical layers) and
29 they have proven to be highly accurate for sandwich stacking sequences. The pioneering
30 works in this field are those by Di Sciuva [8,9] and recent improvements have been
31 proposed by Tessler, Di Sciuva and Gherlone as the **Refined Zigzag Theory** [10,11].
32 The key idea of RZT is to enrich the First-order Shear Deformation Theory by adding a
33 through-the-thickness piecewise linear contribution to the in-plane displacements field.
34 This "zigzag" contribution is built in order to (1) model the normal distortion that is
35 typical of laminated structures and (2) to add only one kinematic variable for the axial
36 displacement assumption to the baseline model. A number of analytical and finite
37 element formulations have been presented for the analysis of one- and two-dimensional
38
39
40
41
42
43
44
45
46
47
48
49
50
51
52
53
54
55
56
57
58
59
60

1
2
3
4
5
6
7
8
9 structures [12-16] and the accuracy of the RZT-based solutions (comparable to that of
10 layer-wise theories) have already been demonstrated for the evaluation of the static
11 response, the free vibration modes and the buckling loads of multilayered composite
12 and sandwich structures.
13
14
15
16

17
18 A large amount of papers available in the open literature deals with the development of
19 theories for the analysis of multilayered sandwich structures. In a vast majority of cases,
20 assessment of these theories is performed through comparison with reference results
21 coming from exact elasticity solutions (when available) or from high-fidelity FE
22 solutions. Very few papers deal with the experimental assessment of theories for the
23 analysis of sandwich structures. In [17], Thomsen and Frostig present the distribution of
24 stresses within sandwich structures under three-point bending measured through photo-
25 elastic experimental procedures; the comparison with the results coming from the
26 HSAPT reveals its capability to model local stress concentrations due to the support and
27 loading systems. Icardi uses electronic speckle photography to experimentally measure
28 the transverse displacement on the free cross-section of a sandwich beam and compares
29 the distribution with the one obtained using a high-order theory [18]. In [19], the linear
30 and geometrically non-linear HSAPT approaches are validated for the four-point
31 bending response prediction of Aluminum-PVC sandwich beams. In [20], the modified
32 couple stress Timoshenko beam theory for sandwich beams with web-cores is assessed
33 through comparison with experimentally measured deflections in three- and four-
34
35
36
37
38
39
40
41
42
43
44
45
46
47
48
49
50
51
52
53
54
55
56
57
58
59
60

1
2
3
4
5
6
7
8
9 bending tests. Typical failure modes of sandwich structures are investigated in [21],
10 namely face yield, core shear and indentation. Three-point bending experiments are
11 conducted on foam-core sandwich beams and failure loads are compared with those
12 obtained using simplified formulas. A good analytical-experimental correlation is found
13 except for the case of thick faces. More recently, experimental tests have been
14 conducted in order to verify the accuracy of the Refined Zigzag Theory in predicting the
15 natural frequencies of sandwich plates [22] and beams [23].
16
17

18
19 The aim of the present effort is to provide an experimental assessment of the RZT also
20 for linear static applications, in particular for the four-point bending of sandwich beams
21 with Aluminum face-sheets and a foam core. Both deflection and axial strain
22 measurements are used for the comparison. Different specimens are tested in order to
23 investigate the effect of geometric and material parameters on the accuracy of RZT.
24
25
26
27
28
29
30
31
32
33
34
35
36
37

38 **2 The Refined Zigzag Theory for beams**

39
40
41
42

43 The **Refined Zigzag Theory** for beams and plates has been extensively described in a
44 number of papers where full details on the kinematic assumptions, derivation of the
45 zigzag function, and governing equations can be found [10,11]. In this section, the
46 fundamental concepts and equations of RZT for beams, together with the solution
47 procedure for the case of four-point bending, are provided in order to set the theoretical
48
49
50
51
52
53
54
55
56
57
58
59
60

and numerical framework of the present study.

2.1 Basic definitions and equations of the theory

A straight beam is referred to a Cartesian coordinate system (x,y,z) , where (x,z) is the plane where deformation is possible and with $x \in [x_a, x_b]$ representing the beam axis and $z \in [-h, h]$ the thickness coordinate (Figure 1). The beam has length $L = x_b - x_a$, thickness $2h$ and cross-sectional area $A = 2h \times b$. N orthotropic, perfectly bonded layers constitute the beam; superscript (k) denotes the generic k th layer.

[INSERT FIGURE 1]

The components of the displacement field of RZT in the (x,z) plane are

$$\begin{aligned} u_x^{(k)}(x, z) &= u(x) + z\theta(x) + \phi^{(k)}(z)\psi(x) \\ u_z(x, z) &= w(x) \end{aligned} \quad (1)$$

where $u_x^{(k)}$ and u_z are the axial and transverse displacements, respectively. RZT for beams is based on four kinematic variables:

- $u(x)$, uniform axial displacement;

- $w(x)$, deflection;
- $\theta(x)$, average cross-section (bending) rotation;
- $\psi(x)$, zigzag rotation.

The displacement field of RZT, Eq. (1), is obtained by adding to the axial displacement of the Timoshenko beam theory a piecewise linear (zigzag), through-the-thickness C^0 -continuous contribution, namely $\phi^{(k)}(z)\psi(x)$. The magnitude of this contribution is measured by the zigzag rotation, $\psi(x)$. The through-the-thickness shape of the contribution is described by the zigzag function, $\phi^{(k)}(z)$, that can be defined in terms of its layer-interface values, ϕ_i ($i = 0, 1, \dots, N$), and is linear with the thickness coordinate, z , within the k th layer between the two values $\phi_{(k-1)}$ and $\phi_{(k)}$

$$\begin{aligned}
 \phi_{(0)} &= 0 && \text{bottom laminate surface} \\
 \phi_{(k)} &= \phi_{(k-1)} + 2h^{(k)}\beta^{(k)} && (k = 1, \dots, N) \\
 \phi_{(N+1)} &= 0 && \text{top laminate surface}
 \end{aligned} \tag{2}$$

In Eq. (2), $2h^{(k)}$ is the thickness of the k th layer and $\beta^{(k)}$ is the zigzag function slope in the same layer ($\beta^{(k)} \equiv \phi_{,z}^{(k)}$). $\beta^{(k)}$ can be calculated as follows

$$\beta^{(k)} = \frac{G}{G_{xz}^{(k)}} - 1 \quad (k = 1, \dots, N) \quad (3)$$

where G represents a zigzag weighted-average transverse shear modulus of the beam cross section

$$G \equiv \frac{2h}{\int_{-h}^h \frac{1}{G_{xz}^{(k)}} dz} \quad (4)$$

and where $G_{xz}^{(k)}$ is the transverse shear modulus of the k th layer.

Within the hypotheses of small displacements and linear strain-displacement relations, the strain field of RZT can be written as

$$\begin{aligned} \varepsilon_x^{(k)}(x, z) &= u_{,x}(x) + z\theta_{,x}(x) + \phi^{(k)}(z)\psi_{,x}(x) \\ \gamma_{xz}^{(k)}(x, z) &= w_{,x}(x) + \theta(x) + \beta^{(k)}\psi(x) \end{aligned} \quad (5)$$

The beam is assumed to exhibit a plane-stress behavior in the (x, z) plane with the orthotropy axes of each layer corresponding to the x - and z -axis. Moreover, the transverse normal stress, $\sigma_z^{(k)}$, can be neglected with respect to the axial and transverse shear ones. Therefore, the constitutive relations of the k th layer read as follows

$$\begin{aligned}\sigma_x^{(k)} &= E_x^{(k)} \varepsilon_x^{(k)} \\ \tau_{xz}^{(k)} &= G_{xz}^{(k)} \gamma_{xz}^{(k)}\end{aligned}\quad (6)$$

where $E_x^{(k)}$ is the Young modulus of the k th layer.

The beam is subject to static loads. Applied at the bottom and top beam surfaces, respectively, $q^b(x)$ and $q^t(x)$ are distributed transverse loads (per unit length). The end cross-sections are subject to the prescribed axial (T_{xa} , T_{xb}) and transverse shear (T_{za} , T_{zb}) tractions. Equilibrium equations of the beam according to RZT can be obtained using the Principle of Virtual Works [10]

$$\begin{aligned}N_{x,x} &= 0 \\ V_{x,x} &= -q(x) \\ M_{x,x} - V_x &= 0 \\ M_{\phi,x} - V_\phi &= 0\end{aligned}\quad (7)$$

where $q \equiv q^b + q^t$ and

$$(N_x, M_x, M_\phi, V_x, V_\phi) \equiv \int_A (\sigma_x^{(k)}, z \sigma_x^{(k)}, \phi^{(k)} \sigma_x^{(k)}, \tau_{xz}^{(k)}, \beta^{(k)} \tau_{xz}^{(k)}) dA \quad (8)$$

are the stress resultants. The Principle of Virtual Works also provides the consistent boundary conditions

$$\left. \begin{aligned} u(x_\alpha) = \bar{u}_\alpha & \quad or & N_x(x_\alpha) = \bar{N}_{x\alpha} \\ w(x_\alpha) = \bar{w}_\alpha & \quad or & V_x(x_\alpha) = \bar{V}_{x\alpha} \\ \theta(x_\alpha) = \bar{\theta}_\alpha & \quad or & M_x(x_\alpha) = \bar{M}_{x\alpha} \\ \psi(x_\alpha) = \bar{\psi}_\alpha & \quad or & M_\phi(x_\alpha) = \bar{M}_{\phi\alpha} \end{aligned} \right\} (\alpha = a, b) \quad (9)$$

where

$$(\bar{N}_{x\alpha}, \bar{M}_{x\alpha}, \bar{M}_{\phi\alpha}, \bar{V}_{x\alpha}) \equiv \int_A (T_{x\alpha}, zT_{x\alpha}, \phi^{(k)}T_{x\alpha}, T_{z\alpha}) dA \quad (\alpha = a, b) \quad (10)$$

are the prescribed-stress resultants at the beam ends. The constitutive equations, expressing the relation between stress resultants and derivatives of the kinematic unknowns, are

$$\begin{aligned} \begin{Bmatrix} N_x \\ M_x \\ M_\phi \end{Bmatrix} &= \begin{bmatrix} A_{11} & B_{12} & B_{13} \\ B_{12} & D_{11} & D_{12} \\ B_{13} & D_{12} & D_{22} \end{bmatrix} \begin{Bmatrix} u_{,x} \\ \theta_{,x} \\ \psi_{,x} \end{Bmatrix} \\ \begin{Bmatrix} V_x \\ V_\phi \end{Bmatrix} &= \begin{bmatrix} \bar{G}A & (G - \bar{G})A \\ (G - \bar{G})A & (\bar{G} - G)A \end{bmatrix} \begin{Bmatrix} w_{,x} + \theta \\ \psi \end{Bmatrix} \end{aligned} \quad (11)$$

where the stiffness coefficients are defined as

$$\begin{aligned}
 (A_{11}, B_{12}, D_{11}) &\equiv \int_A E_x^{(k)} (1, z, z^2) dA \\
 (B_{13}, D_{12}, D_{22}) &\equiv \int_A E_x^{(k)} \phi^{(k)} (1, z, \phi^{(k)}) dA \\
 \bar{G} &\equiv \frac{1}{2h} \int_{-h}^h G_{xz}^{(k)} dz
 \end{aligned} \tag{12}$$

By substituting Eqs. (12) into Eqs. (7), the equilibrium equations expressed in terms of the kinematic variables can be written as

$$\begin{aligned}
 A_{11}u_{,xx} + B_{12}\theta_{,xx} + B_{13}\psi_{,xx} &= 0 \\
 \bar{G}A(w_{,xx} + \theta_{,x}) + (G - \bar{G})A\psi_{,x} &= -q(x) \\
 B_{12}u_{,xx} + D_{11}\theta_{,xx} + D_{12}\psi_{,xx} - \bar{G}A(w_{,x} + \theta) - (G - \bar{G})A\psi &= 0 \\
 B_{13}u_{,xx} + D_{12}\theta_{,xx} + D_{22}\psi_{,xx} - (G - \bar{G})A(w_{,x} + \theta) - (\bar{G} - G)A\psi &= 0
 \end{aligned} \tag{13}$$

Equilibrium equations (13), together with boundary conditions (9), cannot be solved exactly except for some special cases [10]. The usual problem of a beam simply supported on both ends and subject only to transverse load $q(x)$ has an exact, Navier-type solution with the kinematic unknowns expressed as trigonometric series of the axial coordinate. An exact solution can be also found for the case of concentrated forces and moments ($q(x) = 0$, [10]) and, in particular, for the classical four-point bending test.

2.2 Exact solution for four-point bending

In Figure 2(a), the loading and boundary conditions of a beam subjected to a four-point bending test are depicted. By taking advantage of the symmetry conditions, the problem can be solved as in Figure 2(b).

[INSERT FIGURE 2(a)]

[INSERT FIGURE 2(b)]

Within the three spans, $x \in (0, a/2)$, $x \in (a/2, S/2)$ and $x \in (S/2, L/2)$, no distributed loads are applied to the beam ($q(x) = 0$) and Eqs. (13) have a solution for each span in the form [10]

$$\begin{aligned}
 u(x) &= \left(-C_8 + C_3 C_7 - \frac{C_2 C_7}{R^2 D_{11}^*} \right) (a_1 \cosh(Rx) + a_2 \sinh(Rx)) - \frac{C_2 C_7 a_3}{2 D_{11}^*} x^2 + a_6 x + a_7 \\
 w(x) &= \left[\frac{C_3}{R} - \frac{C_2}{R^3 D_{11}^*} + \frac{1}{R} \left(\frac{C_2 C_5}{D_{11}^*} - C_4 \right) + R(C_6 - C_3 C_5) \right] (a_1 \sinh(Rx) + a_2 \cosh(Rx)) \\
 &\quad - \frac{C_2 a_3}{6 D_{11}^*} x^3 - \frac{a_4}{2} x^2 + \left[\left(\frac{C_2 C_5}{D_{11}^*} - C_4 \right) a_3 - a_5 \right] x + a_8 \\
 \theta(x) &= \left(-C_3 + \frac{C_2}{R^2 D_{11}^*} \right) (a_1 \cosh(Rx) + a_2 \sinh(Rx)) + \frac{C_2 a_3}{2 D_{11}^*} x^2 + a_4 x + a_5 \\
 \psi(x) &= a_1 \cosh(Rx) + a_2 \sinh(Rx) + a_3
 \end{aligned} \tag{14}$$

where C_i ($i=1,\dots,8$), D_{11}^* and R are functions of the stiffness coefficients defined in Eqs. (12) (see [24]) whereas the a_i ($i=1,\dots,8$) unknown constants are determined from the boundary conditions, Eqs. (9). Since, in the present case, three spans have to be considered, there are 24 a_i constants to be determined by using the following 24 boundary conditions

$$\begin{aligned}
 x=0 & \begin{cases} u=0 \\ V_x=0 \\ \theta=0 \\ \psi=0 \end{cases} \\
 x=a/2 & \begin{cases} u^- = u^+ & N_x^- = N_x^+ \\ w^- = w^+ & V_x^- + F/2 = V_x^+ \\ \theta^- = \theta^+ & M_x^- = M_x^+ \\ \psi^- = \psi^+ & M_\phi^- = M_\phi^+ \end{cases} \\
 x=S/2 & \begin{cases} u^- = u^+ & N_x^- = N_x^+ \\ w^- = w^+ & w^- = 0 \\ \theta^- = \theta^+ & M_x^- = M_x^+ \\ \psi^- = \psi^+ & M_\phi^- = M_\phi^+ \end{cases} \\
 x=L/2 & \begin{cases} N_x=0 \\ V_x=0 \\ M_x=0 \\ M_\phi=0 \end{cases}
 \end{aligned} \tag{15}$$

where superscripts – and + denote, respectively, the left and right side of the beam cross

1
2
3
4
5
6
7
8
9 section for the internal stations ($x = a/2$ and $x = S/2$). Once the 24 a_i constants have
10
11 been evaluated, the distribution of the kinematic unknowns, $u(x)$, $w(x)$, $\theta(x)$ and
12
13 $\psi(x)$, is determined in each span (see Eq. (14)) and it is then possible to calculate
14
15 strains and stresses (Eqs. (5) and (6)).
16
17

18 For the special case with $S = L$ and $a = L/2$, an explicit formula for the maximum
19
20 deflection, $w(x = 0)$, has been derived and presented in [25]. For the present case, no
21
22 explicit expressions for displacements, strains, and stresses are provided but the solution
23
24 of Eqs. (14) and (15) have been implemented numerically.
25
26
27
28
29

30 **3 Bending experiments on sandwich beams**

31
32
33
34

35 This paragraph is devoted to the description of the experimental campaign performed on
36
37 sandwich beams. The experiments have been conducted at the LAQ-AERMEC
38
39 laboratory of the Mechanical and Aerospace Engineering Department of the Politecnico
40
41 di Torino, whereas the specimens have been manufactured by the AMATECH
42
43 laboratory of the Aerospace Science and Technology Department of Politecnico di
44
45 Milano.
46
47
48
49
50
51
52
53
54
55
56
57
58
59
60

3.1 Specimens

The sandwich beams considered for the experimental activity are made by a 7075 Aluminum alloy and Rohacell[®] cores. Both materials find wide application in aircraft structures and Rohacell[®] is in particular used as core within helicopter rotor blades, body panels of rockets and stringer structures in the pressure bulkheads of civil transport aircrafts [26]. The thickness of each of the two face-sheets is h_f whereas the thickness of the core is h_c . The total thickness is $2h=2h_f+h_c$. In order to investigate the effect of the mechanical properties of the core, two types of structural foams have been considered, namely the IG31 and the WF110 [26]. Moreover, in order to investigate the effect of the supported length-to-thickness ratio ($S/2h$) and the face-to-core thickness ratio (h_f/h_c), several geometries have been considered. In Table 1, each specimen is denoted with its nomenclature and dimensions, (average values of three measures in different position along the beam length).

Table 1. Specimens nomenclature and measured geometry (see Figure 2(a)).

Specimen	L (mm)	S (mm)	b (mm)	h_f (mm)	h_c (mm)	h_f/h_c	$S/2h$
IG31_32_5	359	321	48.3	5.00	5.88	0.85	20.21
WF110_32_5	360	321	48.3	5.00	6.07	0.82	19.98
WF110_64_5	680	640	48.3	5.00	6.13	0.82	39.68
IG31_48_2	520	480	72.2	2.00	19.90	0.10	20.08
WF110_48_2	520	481	72.2	2.00	20.07	0.10	19.98
IG31_44_1	480	441	66.1	1.05	19.50	0.05	20.42

3.2 Material characterization

In order to perform a reliable comparison between the numerical results and the experimental ones, an accurate mechanical characterization of 7075 Aluminum alloy and Rohacell[®] foams is necessary.

The Young's modulus and the Poisson's ratio of the 7075 Aluminum alloy have been evaluated in compliance with the ASTM 857M and E 111 standards [27,28]. Figure 3 shows one of the stress-strain curves obtained during the characterization: three different Aluminum specimens have been tested and the average values of E and ν have been computed.

[INSERT FIGURE 3]

1
2
3
4
5
6
7
8
9
10
11 The Rohacell[®] material characterization has been performed by means of some
12 experimental tests and numerical correlations with high-fidelity FE models (refer to [29]
13 for a detailed description of the whole procedure). The Young modulus of the core
14 materials has been evaluated by performing three-point bending tests on six foam
15 specimens (three for IG31 and three for WF110, see Figure 4) where two deflections
16 have been measured: at the beam mid-span and at one quarter of its length. The same
17 bending tests have been numerically simulated with MSC/NASTRAN: two-dimensional
18 plane-stress models discretized with QUAD8 elements have been used where the core
19 Young modulus and shear modulus have been parametrically varied. Due to the
20 specimens' dimensions (slenderness = 10), the transverse shear deformability has given
21 negligible contribution to the overall deformation, thus numerical results were
22 influenced by the Young's modulus only and were insensitive to the shear modulus. By
23 matching the FE results with the experimental ones, it has been possible to evaluate the
24 Young modulus of both IG31 and WF110 foam (Table 2). The effect of the core shear
25 modulus can be measured if the test is on a sandwich beam whose transverse shear
26 deformability strongly affects the global deformation. Therefore, the foam material
27 shear modulus has been evaluated considering the IG_32_5 and WF_32_5 four-point
28 bending tests (see Section 3.3) and corresponding MSC/NASTRAN plane-stress models
29 (with faces and core Young moduli set to the already measured values, Table 2). The
30
31
32
33
34
35
36
37
38
39
40
41
42
43
44
45
46
47
48
49
50
51
52
53
54
55
56
57
58
59
60

1
2
3
4
5
6
7
8
9 core shear modulus has been selected as the one that leads to the best correspondence
10
11 between the experimentally measured and the numerically evaluated deflections.
12
13

14
15 *[INSERT FIGURE 4]*
16

17
18
19 In Table 2, the nominal properties of the Aluminum alloy and of the Rohacell[®] foams
20
21 are compared with those obtained by the characterization process: due to the number of
22
23 specimens used for the foam Young's modulus characterization, the results are given in
24
25 terms of average value and standard deviation.
26
27
28
29
30
31
32
33
34
35
36
37
38
39
40
41
42
43
44
45
46
47
48
49
50
51
52
53
54
55
56
57
58
59
60

Table 2. Material mechanical properties: nominal and characterized values of Young modulus, E, and shear modulus, G. Results for the Aluminum alloy are expressed in terms of E and G even if the Poisson's ratio has been directly experimentally evaluated. Since the measured values of E and G for the Rohacell® cores do not satisfy the condition of positive definition of the matrix of elastic coefficients of an isotropic material, for which $\nu = E/2G - 1 < 0.5$, the materials have been assumed to behave as orthotropic with $E_i = E$, $G_{ij} = G$ and $\nu = 0.3$.

Material	Nominal		Characterized	
	E (MPa)	G (MPa)	E (MPa)	G (MPa)
7075 Aluminum alloy	73000	28077	69570	25766
Rohacell® IG31	36	13	40.3±4.9	12.4
Rohacell® WF110	180	70	196±8.6	65.4

3.3 Four-point bending test: experimental set-up

The four-point bending test on sandwich beams of Table 1 has been performed on the universal testing machine METROCOM (see Figure 5) equipped with two **inductive displacement transducers** (HBM - WI ± 2.5 mm), a load cell (HBM - Strain Gage Load Cell, 200 kg) and a load transmission system (two cylinders connected to the load cell by means of a rigid plate). Transverse displacement has been measured in two positions along the beam axis using the **displacement transducers**, the axial strain has been

1
2
3
4
5
6
7
8
9 measured in different locations by using strain gages located on the top and bottom
10 external beam surfaces. The positions of the displacement transducers and of the strain
11 gages are depicted in Figure 6. The distance between the two load cylinders (Figure
12 2(a)) and between the central and lateral strain gages (Figure 6) is $a=110\text{ mm}$. The test
13 on beams IG_44_1, IG_48_2, WF_48_2 and WF_64_5 has been conducted with all of
14 the three strain gages. Once verified that the two strain gages co-located at the beam
15 mid-span provided fairly opposite measurements, only one central strain gage has been
16 used for the IG_32_5 and WF_32_5 specimens. The reduced length of the latter beams
17 also led to skipping the lateral strain gage. The test has been performed in displacement
18 control at a rate of 0.01 mm/sec (the controlled displacement is w_c).

19
20
21
22
23
24
25
26
27
28
29
30
31
32
33 *[INSERT FIGURE 5]*

34
35
36
37
38 *[INSERT FIGURE 6]*

39 40 41 42 **4 Results and discussion**

43
44
45
46
47 In this section, the experimental results obtained by the test described in the previous
48 paragraph are collected and compared with the numerical results obtained using the
49 RZT analytical solution presented in Sect. 2.2. Moreover, to enrich the comparison and
50
51
52
53
54
55
56
57
58
59
60

to evaluate the enhancements ensured by RZT, the results coming from the Timoshenko Beam Theory (TBT), adopting an ad-hoc shear correction factor, are included. The shear correction factor has been calculated according to [30] and the solution of the four-bending test has been obtained following a procedure similar to the one described in Sect. 2.2 for RZT.

Experimental results are collected in Table 3. The RZT and TBT results are given in Figure 7 in terms of relative percent error with respect to the experimental measurements.

Table 3. Experimental results.

	$100 \cdot w_m / F$ (mm/kg)	$100 \cdot w_c / F$ (mm/kg)	ε_{\max}^B / F ($\mu\varepsilon/\text{kg}$)	ε_{\max}^T / F ($\mu\varepsilon/\text{kg}$)	$\varepsilon_{\text{lat}}^T / F$ ($\mu\varepsilon/\text{kg}$)
IG_32_5	2.79	2.48	7.38	/	/
WF_32_5	1.13	0.99	4.40	/	/
WF_64_5	6.22	5.81	10.19	-9.98	-8.33
IG_48_2	4.52	4.34	4.57	-4.79	-3.48
WF_48_2	1.70	1.60	4.45	-4.53	-3.33
IG_44_1	5.70	5.48	8.23	-8.78	-5.79

1
2
3
4
5
6
7
8
9
10
11
12
13
14
15
16
17
18
19
20
21
22
23
24
25
26
27
28
29
30
31
32
33
34
35
36
37
38
39
40
41
42
43
44
45
46
47
48
49
50
51
52
53
54
55
56
57
58
59
60

[INSERT FIGURE 7(a)]

[INSERT FIGURE 7(b)]

[INSERT FIGURE 7(c)]

[INSERT FIGURE 7(d)]

[INSERT FIGURE 7(e)]

[INSERT FIGURE 7(f)]

The TBT results show a clear trend: the error increases by increasing the cross-section heterogeneity, that is by increasing the face-to-core stiffness ratio (greater for the beam with the IG31 core and lower for the WF110 foam), and by increasing the face-to-core thickness ratio. The errors are up to the 70% on the deflection and up to the 48% on the strain, even if an ad-hoc shear correction factor is used. On the contrary, the error decreases by increasing the length-to-thickness ratio, as a result of a reduced transverse shear deformability contribution to the total beam deflection.

On the contrary, the RZT results appears substantially more accurate than the TBT ones, with a maximum error up to the 7.3% on the deflection and up to 10% on the longitudinal strain. With respect to the TBT model, the RZT is able to accurately reproduce the transverse shear strain contribution that becomes significant in sandwich beams with high face-to-core stiffness ratio, relevant face-to-core thickness ratio and for beams with reduced slenderness. Moreover, the comparison between the RZT results and the TBT ones demonstrates the greatest improvement achievable by enriching the TBT kinematics with the RZT zigzag contribution, rather than using a shear correction factor.

1
2
3
4
5
6
7
8
9 Generally speaking, the errors relative to the specimens adopting the IG31 core are
10 higher than those relative to the beams with the WF110 core. This is due to the
11 mechanical properties dispersion: in Table 2, the standard deviation of the IG31
12 Young's modulus is around the 12% of the average value, contrary to the 4% of the
13 WF110. This leads to a greater error on the results relative to the IG31 specimens.
14
15 Moreover, it is worth to note that, in these analyses, the effect of the thin adhesive layer
16 has been neglected: investigation about the effect of the adhesive layer is in progress.
17

18
19 Finally, in order to highlight that the considered sandwich beams represent challenging
20 problems due to the complexity of their mechanical response, we focus on beams
21 WF_32_5 and WF_64_5. Figures 8 and 9 are related to beam WF_32_5 and show,
22 respectively, the deflection shape on half of the geometry (according to Figure 2(b)) and
23 the through-the-thickness distribution of the axial strain for $x=0$. Similarly, Figures 10
24 and 11 show the response of beam WF_64_5. Results obtained using RZT and TBT are
25 compared and the available experimental measurements are also shown. It is in
26 particular interesting the “zigzag” pattern of the axial strain distribution (more
27 pronounced for the less slender beam WF_32_5) and the effect that this shape has on
28 the maximum values that can be measured on top and bottom laminate faces. The
29 Refined Zigzag Theory provides an accurate esteem of these extreme values.
30
31
32
33
34
35
36
37
38
39
40
41
42
43
44
45
46
47
48
49
50

51 **[INSERT FIGURE 8]**
52
53
54
55
56
57
58
59
60

1
2
3
4
5
6
7
8
9
10
11 *[INSERT FIGURE 9]*
12
13

14
15 *[INSERT FIGURE 10]*
16
17

18
19 *[INSERT FIGURE 11]*
20
21
22
23

24 **5 Conclusions**

25
26
27
28
29 The paper describes an experimental campaign conducted to assess the **Refined Zigzag**
30 **Theory** and its modeling capabilities of sandwich beams under static bending.
31
32

33
34 The kinematic assumptions and governing equations of RZT for one-dimensional
35 problems are briefly reviewed and an analytic solution for beams in four-point-bending
36 boundary and loading conditions is derived. The first phase of the experimental
37 campaign aims at the material mechanical characterization. The material of face-sheets
38 is an Aluminum alloy whereas the core is a structural polymeric foam (Rohacell®).
39
40 Then, four-point bending tests are conducted on beams with different values of
41 slenderness, face-to-core thickness and face-to-core stiffness ratios. The beam
42 deflection is measured at two different positions and the axial strain is measured at three
43 locations on the external surfaces.
44
45
46
47
48
49
50
51
52
53
54
55
56
57
58
59
60

1
2
3
4
5
6
7
8
9
10
11
12
13
14
15
16
17
18
19
20
21
22
23
24
25
26
27
28
29
30
31
32
33
34
35
36
37
38
39
40
41
42
43
44
45
46
47
48
49
50
51
52
53
54
55
56
57
58
59
60

Experimental results are compared with those coming from the analytic RZT solution and with those obtained likewise using the **Timoshenko Beam Theory** with an ad-hoc shear correction factor. The analysis of results reveals that RZT is more accurate than TBT especially for short beams and when the face-to-core thickness and stiffness ratios are higher. This is appreciable not only for global response predictions (deflection) but also for local quantities such as axial strains, in particular when their through-the-thickness distribution exhibit a zigzag pattern.

The present paper represents a further effort towards a complete experimental assessment of the Refined Zigzag Theory. Future steps within this path will be dedicated to buckling loads and to the effect of adhesive layers on the global and local responses of sandwich beams.

Acknowledgement

The authors acknowledge **Juan Eduardo Lawrie**, Daniela Ferrucci and Alessandro Siracusa for their help during the experimental activity which was part of their thesis activity for a master degree in Aerospace Engineering.

References

- [1] Noor AK and Burton CW. Computational models for sandwich panels and shells. *App Mech Rev* 1996; 49: 155–199.
- [2] Hohe J and Becker W. A refined analysis of the effective elasticity tensor for general cellular sandwich cores. *Int J Solids Struct* 2001; 38: 3689–3717.
- [3] Reddy JN. A generalization of two-dimensional theories of laminated composite plates. *Comm Appl Num Meth* 1987; 3(3): 173–180.
- [4] Librescu L, Khdeir A and Reddy JN. A comprehensive analysis of the state of stress of elastic anisotropic flat plates using refined theories. *Acta Mech* 1987; 70: 57–81.
- [5] Plantema FJ. *Sandwich construction: the bending and buckling of sandwich beams, plates, and shells*. John Wiley & Sons, 1966.
- [6] Allen HG. *Analysis and design of structural sandwich panels*. Pergamon, 1969.
- [7] Frostig Y, Baruch M, Vilnay O and Sheinman I. High-order theory for sandwich-beam behavior with transversely flexible core. *J Eng Mech* 1992; 118(5): 1026–1043.
- [8] Di Sciuva M. Development of an anisotropic, multilayered, shear-deformable rectangular plate element. *Comput Struct* 1985; 21(4): 789–796.
- [9] Di Sciuva M. Multilayered anisotropic plate models with continuous interlaminar

- 1
2
3
4
5
6
7
8 stresses. *Compos Struct* 1992; 22(3): 149–167.
- 9
10
11 [10] Tessler A, Di Sciuva M and Gherlone M. A Refined Zigzag beam Theory for
12 composite and sandwich beams. *J Compos Mat* 2009; 43(9): 1051–1081.
- 13
14
15 [11] Tessler A, Di Sciuva M and Gherlone M. A consistent refinement of First-order
16 Shear-Deformation Theory for laminated composite and sandwich plates using
17 improved zigzag kinematics. *J Mech Mat Struct* 2010; 5(2): 341–367.
- 18
19
20 [12] Gherlone M, Tessler A and Di Sciuva M. C^0 beam elements based on the Refined
21 Zigzag Theory for multilayered composite and sandwich laminates. *Compos*
22 *Struct* 2011; 93(11): 2882–2894.
- 23
24
25 [13] Oñate E, Eijo A and Oller S. Simple and accurate two-noded beam element for
26 composite laminated beams using a refined zigzag theory. *Comp Meth App Mech*
27 *Eng* 2012; 213–216: 362–382.
- 28
29
30 [14] Iurlaro L, Gherlone M, Di Sciuva M and Tessler A. Assessment of the Refined
31 Zigzag Theory for bending, vibration, and buckling of sandwich plates: a
32 comparative study of different theories. *Compos Struct* 2013; 106: 777–792.
- 33
34
35 [15] Versino D, Mattone M, Gherlone M, Tessler A and Di Sciuva M. An efficient, C^0
36 triangular element based on the Refined Zigzag Theory for multilayered
37 composite and sandwich plates. *Compos Part B-Eng* 2013; 44B(1): 218–230.
- 38
39
40 [16] Eijo A, Oñate E and Oller S. Delamination in laminated plates using the 4-noded
41 quadrilateral QLRZ plate element based on the Refined Zigzag Theory. *Compos*
42
43
44
45
46
47
48
49
50
51
52
53
54
55
56
57
58
59
60

- 1
2
3
4
5
6
7
8
9
10
11
12
13
14
15
16
17
18
19
20
21
22
23
24
25
26
27
28
29
30
31
32
33
34
35
36
37
38
39
40
41
42
43
44
45
46
47
48
49
50
51
52
53
54
55
56
57
58
59
60
- Struct* 2014; 108: 456–471.
- [17] Thomsen OT and Frostig Y. Localized bending effects in sandwich panels: photoelastic investigation versus high-order sandwich theory results. *Compos Struct* 1997; 37(1): 97–108.
- [18] Icardi U. Through-the-thickness displacements measurement in laminated composites using electronic speckle photography. *Mech Mat* 2003; 35: 35–51.
- [19] Sokolinsky VS, Shen H, Vaikhanski S and Nutt SR. Experimental and analytical study of nonlinear bending response of sandwich beams. *Compos Struct* 2003; 60: 219–229.
- [20] Romanoff J and Reddy JN. Experimental validation of the modified couple stress Timoshenko beam theory for web-core sandwich panels. *Compos Struct* 2014; 111: 130–137.
- [21] Jiang B, Li Z and Lu F. Failure mechanism of sandwich beams subjected to three-point bending. *Compos Struct* 2015; 133: 739–745.
- [22] Honda S, Kumagai T, Tomihashi K and Narita Y. Frequency maximization of laminated sandwich plate under general boundary condition using layerwise optimization method with refined zigzag theory. *J Sound Vib* 2013; 332: 6451–6462.
- [23] Iurlaro L, Ascione A, Gherlone M, Mattone M and Di Sciuva M. Free vibration analysis of sandwich beams using the Refined Zigzag Theory: an experimental

- 1
2
3
4
5
6
7
8
9 assessment. *Mecc* 2015; 50: 2525–2535.
- 10
11 [24] Tessler A, Di Sciuva M and Gherlone M. Refinement of Timoshenko beam theory
12 for composite and sandwich beams using zigzag kinematics. NASA/TP-2007-
13 215086, November 2007.
- 14
15
16
17 [25] Gherlone M. Exact formulas for bending of sandwich beams using the Refined
18 Zigzag Theory. In: *Proceedings of the XI World Congress on Computational*
19 *Mechanics*, Barcelona, Spain, July 20-25 2014.
- 20
21
22
23
24 [26] www.rohacell.com
- 25
26 [27] ASTM 857M. *Standard test methods of tension testing wrought and cast*
27 *Aluminum and Magnesium alloy products (metric)*. ASTM International, 2015.
- 28
29 [28] ASTM E111. *Standard test method for Young's modulus, tangent modulus and*
30 *chord modulus*. ASTM International, 2010.
- 31
32
33
34 [29] Iurlaro L. *Development of refined models for multilayered composite and*
35 *sandwich structures: analytical formulation, FEM implementation and*
36 *experimental assessment*. Ph.D. thesis, Politecnico di Torino, 2015.
- 37
38
39
40 [30] Madabhusi-Raman P and Davalos GF. Static shear correction factors for
41 laminated rectangular beams. *Compos Part B-Eng* 1996; 27B: 285–293.
- 42
43
44
45
46
47
48
49
50
51
52
53
54
55
56
57
58
59
60

Figure Captions

Figure 1. Notation, geometry and loads of the beam.

Figure 2. Notation, geometry and loads of the four-point bending problem: (a) complete problem definition, (b) problem defined on half geometry due to symmetry conditions.

Figure 3. Stress-strain curve for the 7075 Aluminum alloy.

Figure 4. Rohacell[®] three-point bending test: A. rigid frame; B. displacement-control system; C. load cell; D., E. displacement transducers.

Figure 5. Four-point bending test, experimental set-up: A. supports, B. loading system, C. load cell, D. displacement transducers.

Figure 6. Position of displacement transducers (measuring w_m and w_c) and strain gages (measuring ε_{\max}^B , ε_{\max}^T and ε_{lat}^T).

Figure 7. Percent errors of the RZT and TBT analytical solutions with respect to the experimental results (the shear correction factor, k^2 , used in the TBT analysis is provided for each case): (a) IG_32_5, (b) WF_32_5, (c) WF_64_5, (d) IG_48_2, (e) WF_48_2, (f) IG_44_1.

Figure 8. Beam WF_32_5, deflection shape on half of the geometry (see Figure 2(b)).

Figure 9. Beam WF_32_5, through-the-thickness distribution of the axial strain for $x=0$.

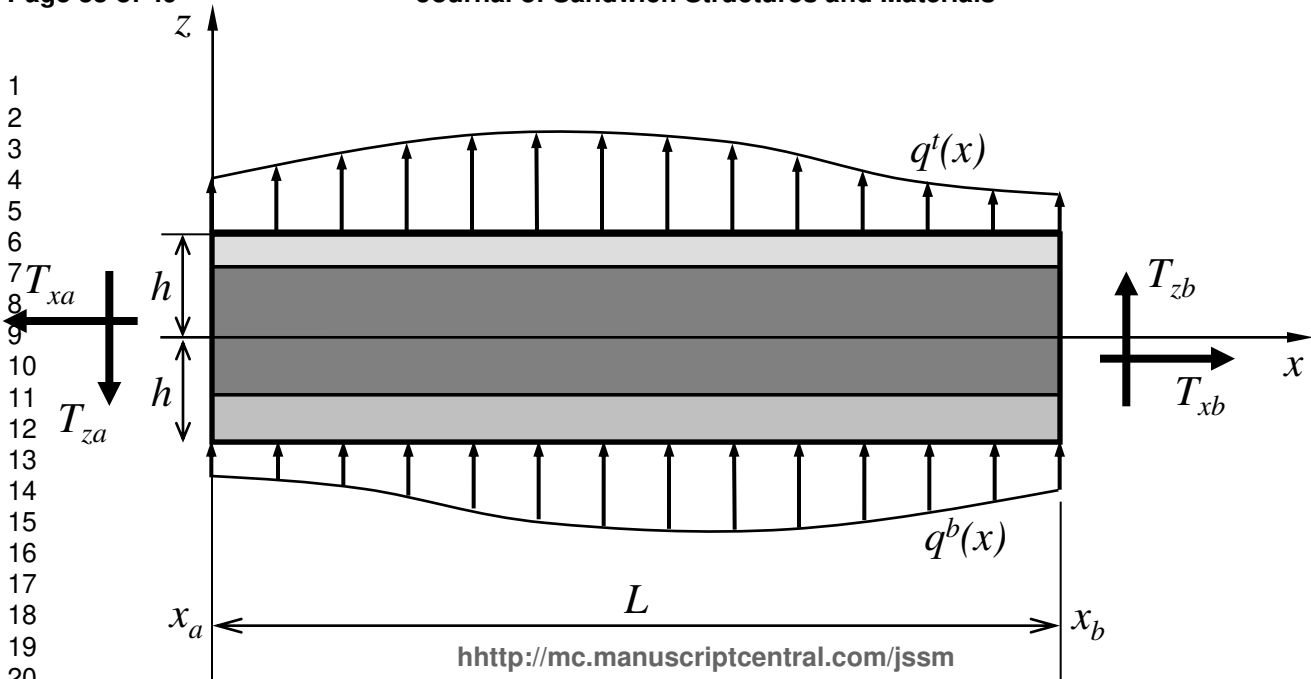
Figure 10. Beam WF_64_5, deflection shape on half of the geometry (see Figure 2(b)).

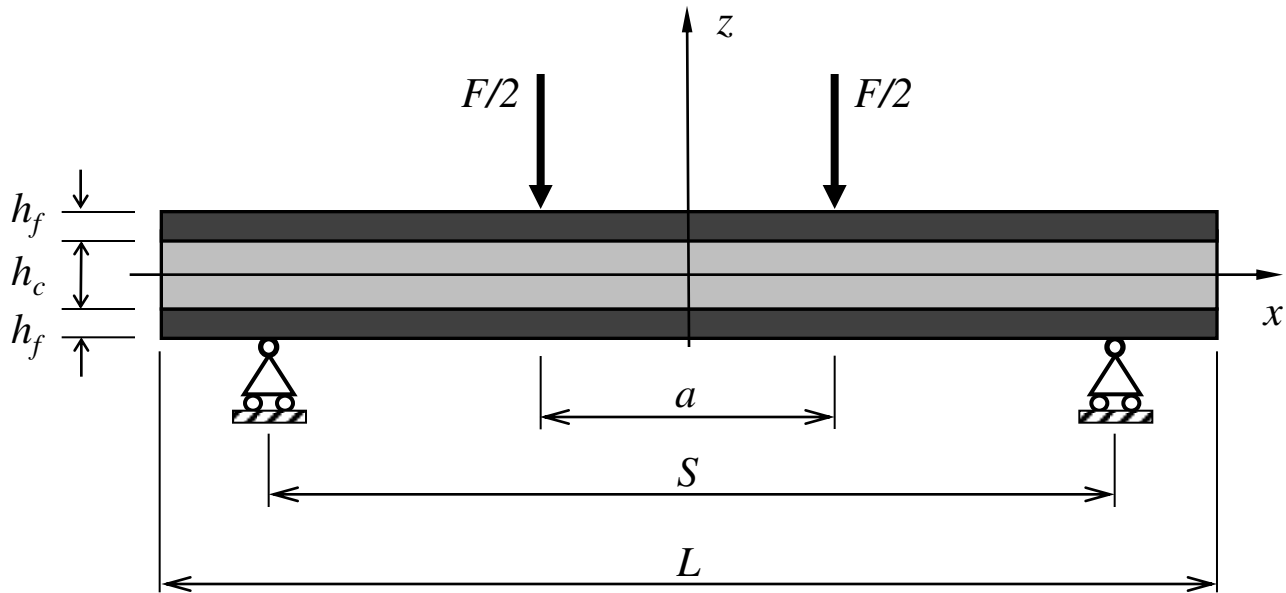
1
2
3
4
5
6
7
8
9 **Figure 11.** Beam WF_64_5, through-the-thickness distribution of the axial strain for
10
11 $x=0$.

12
13
14
15
16
17
18
19
20
21
22
23
24
25
26
27
28
29
30
31
32
33
34
35
36
37
38
39
40
41
42
43
44
45
46
47
48
49
50
51
52
53
54
55
56
57
58
59
60

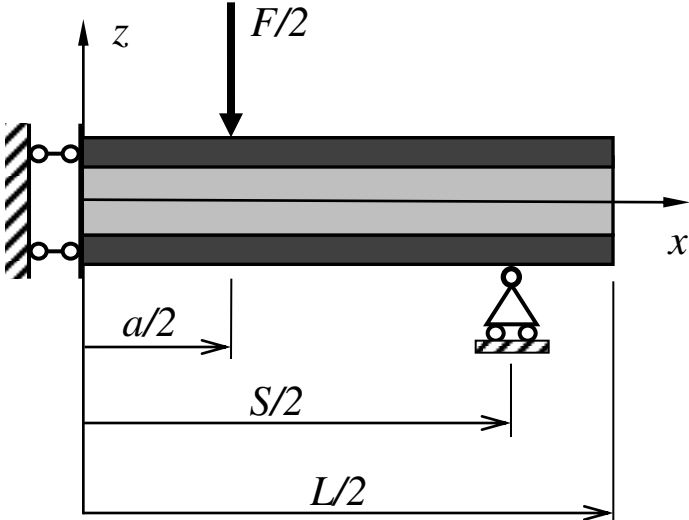
For Peer Review

1
2
3
4
5
6
7
8
9
10
11
12
13
14
15
16
17
18
19
20
21
22

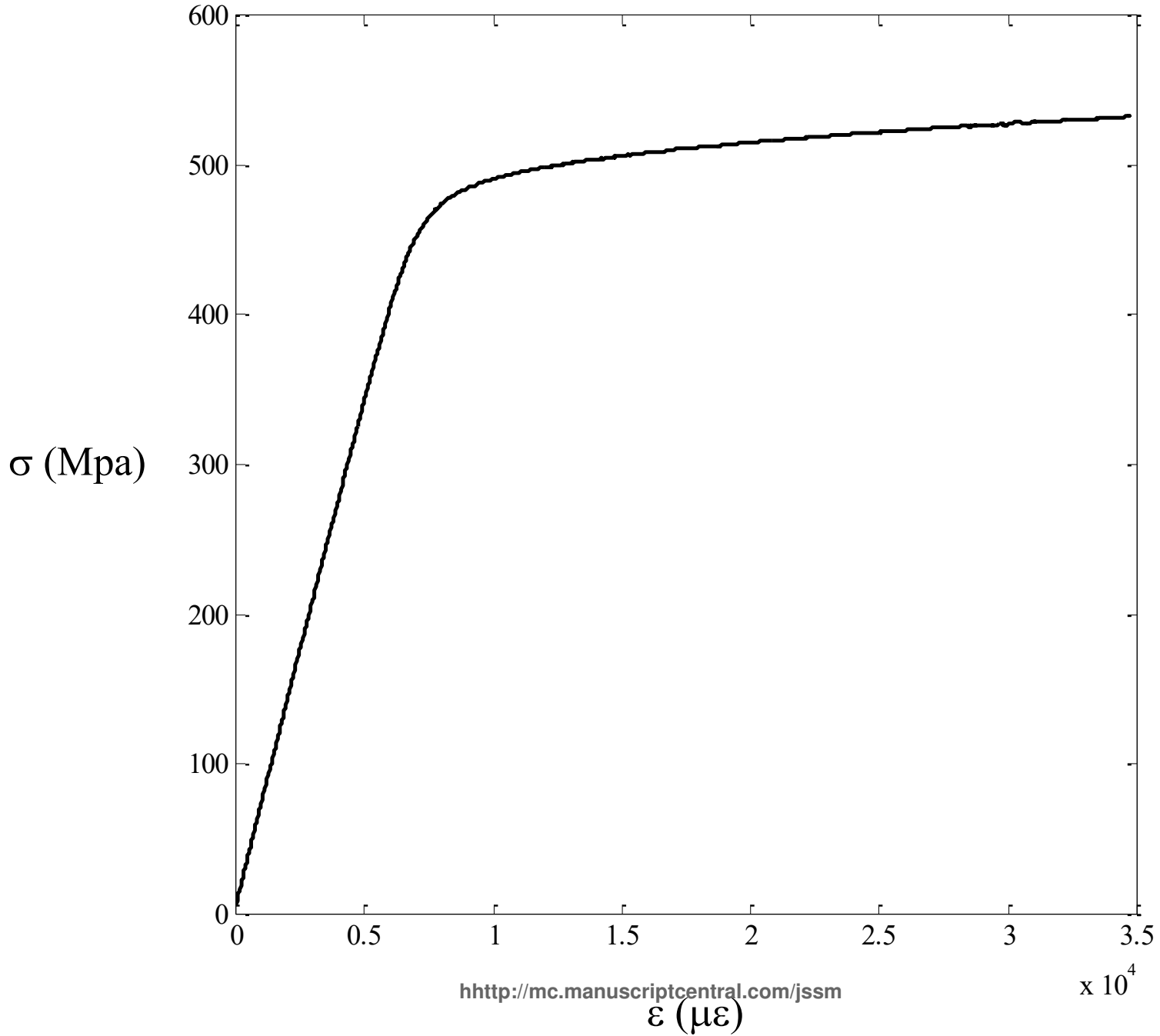




1
2
3
4
5
6
7
8
9
10
11
12
13
14
15
16
17
18
19
20
21
22



<http://mc.manuscriptcentral.com/jssm>

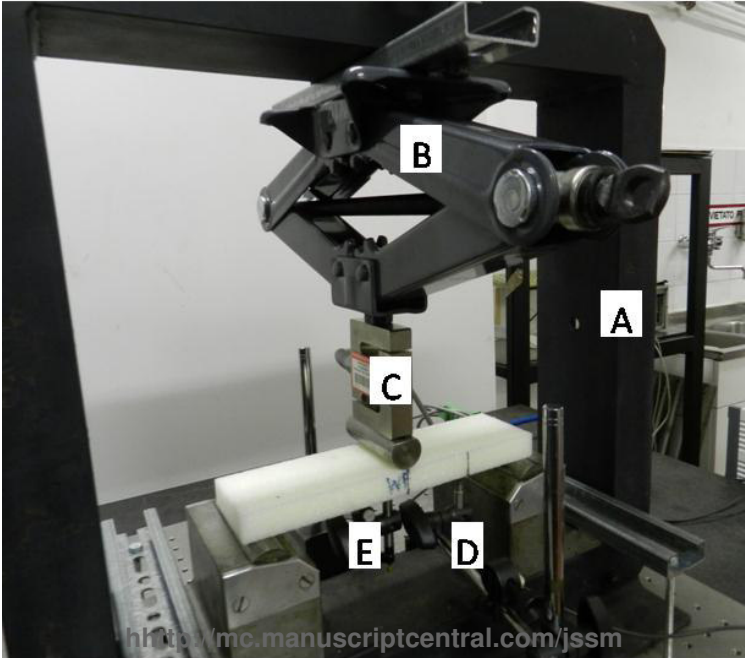


<http://mc.manuscriptcentral.com/jssm>

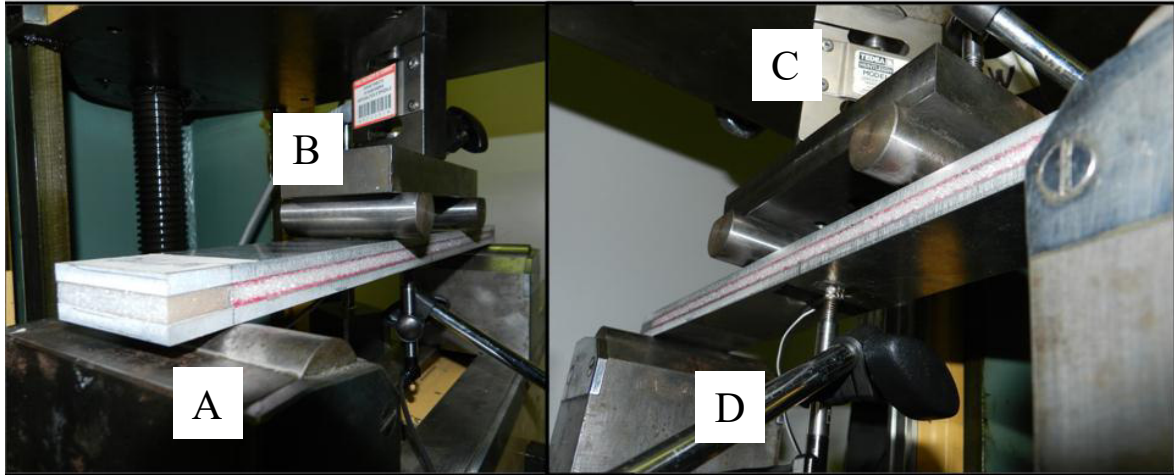
$\times 10^4$

1
2
3
4
5
6
7
8
9
10
11
12
13
14
15
16
17
18
19
20
21
22
23
24
25
26
27
28
29
30
31
32
33
34
35
36
37
38
39
40
41
42
43

1
2
3
4
5
6
7
8
9
10
11
12
13
14
15
16
17
18
19
20
21
22



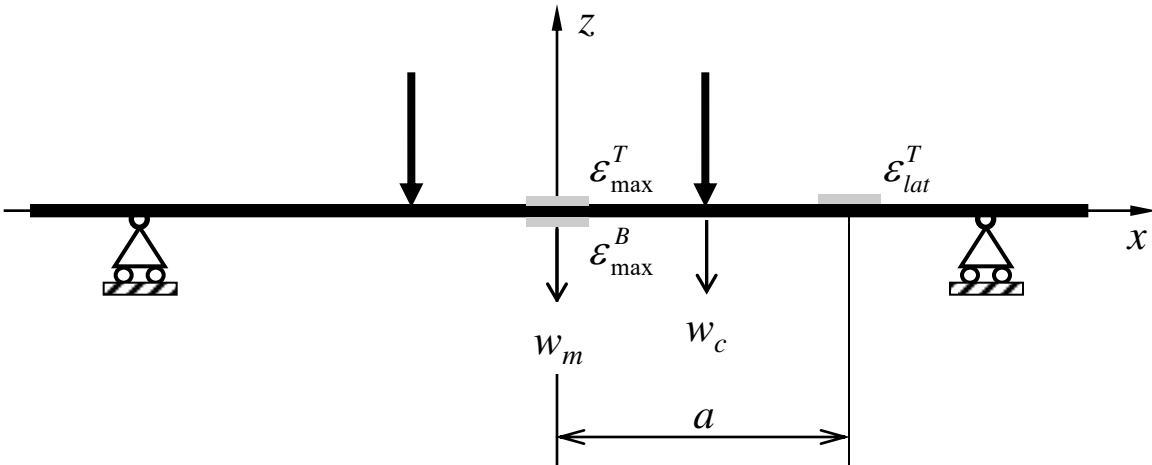
<http://mc.manuscriptcentral.com/jssm>

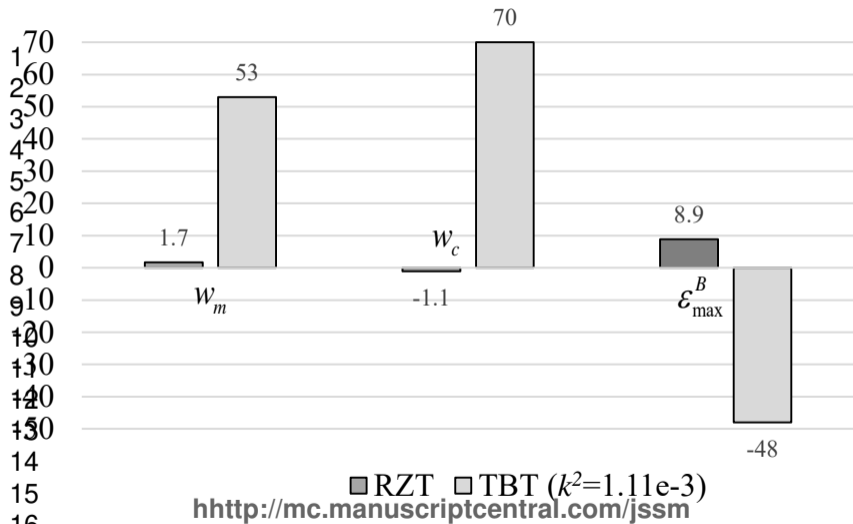


<http://mc.manuscriptcentral.com/jssm>

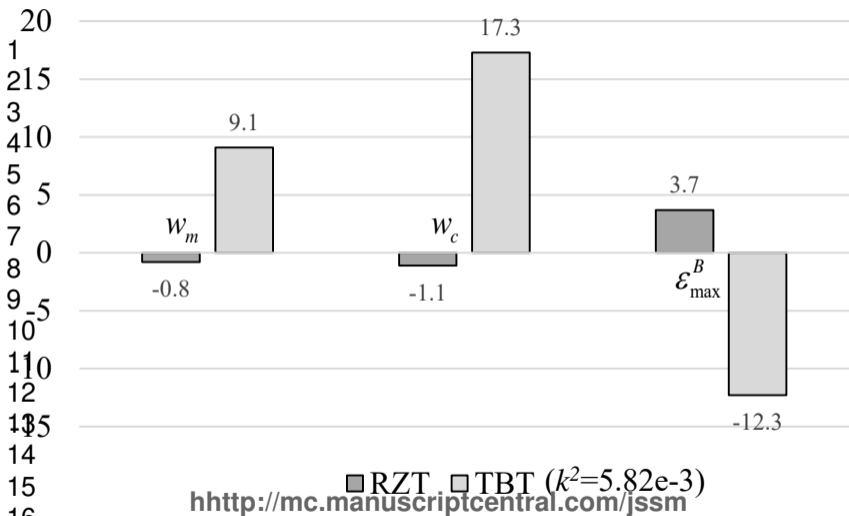
1
2
3
4
5
6
7
8
9
10
11
12
13
14
15
16
17
18
19
20
21
22

1
2
3
4
5
6
7
8
9
10
11
12
13
14
15
16
17
18
19
20
21
22



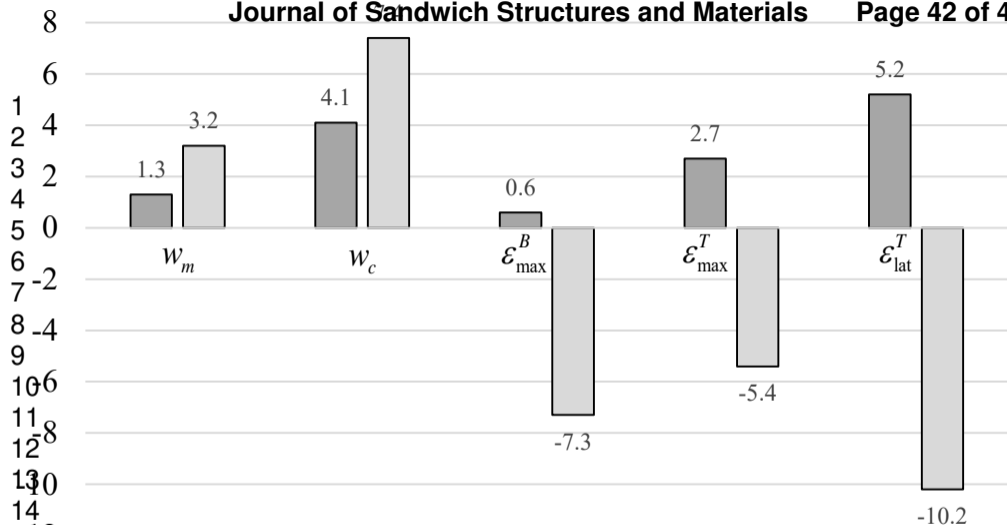


17
18



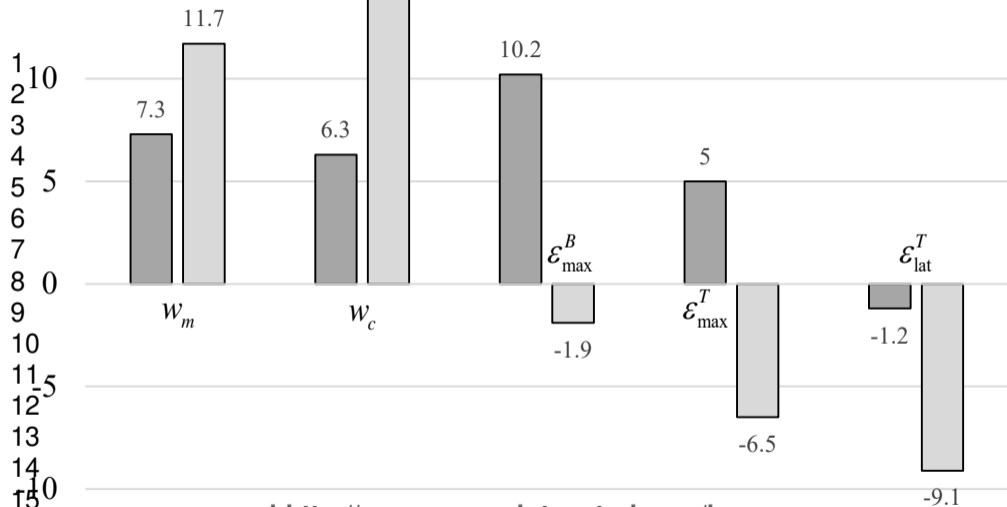
17

18



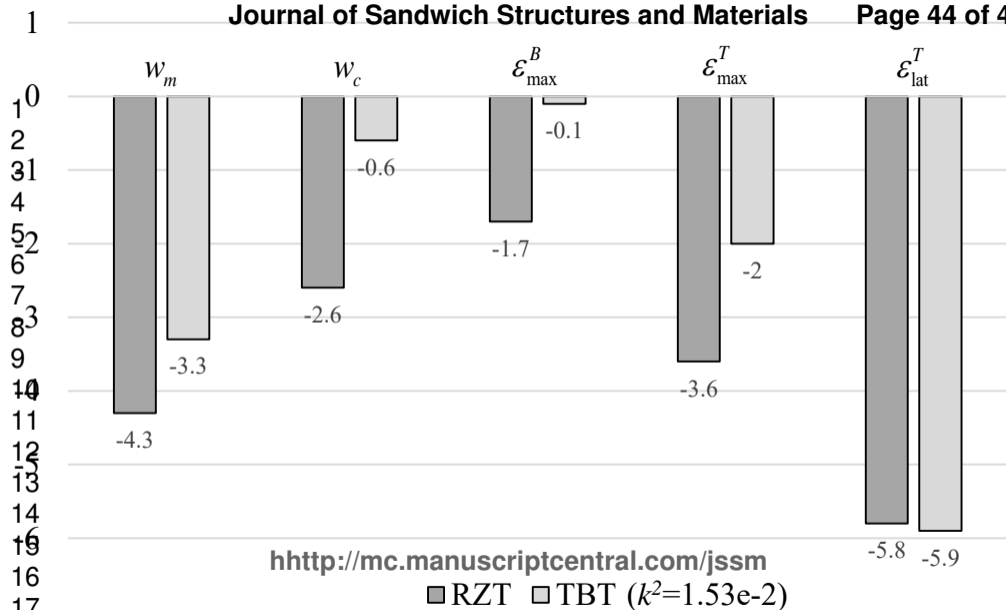
<http://mc.manuscriptcentral.com/jssm>

■ RZT ■ TBT ($k^2=5.82e-3$)



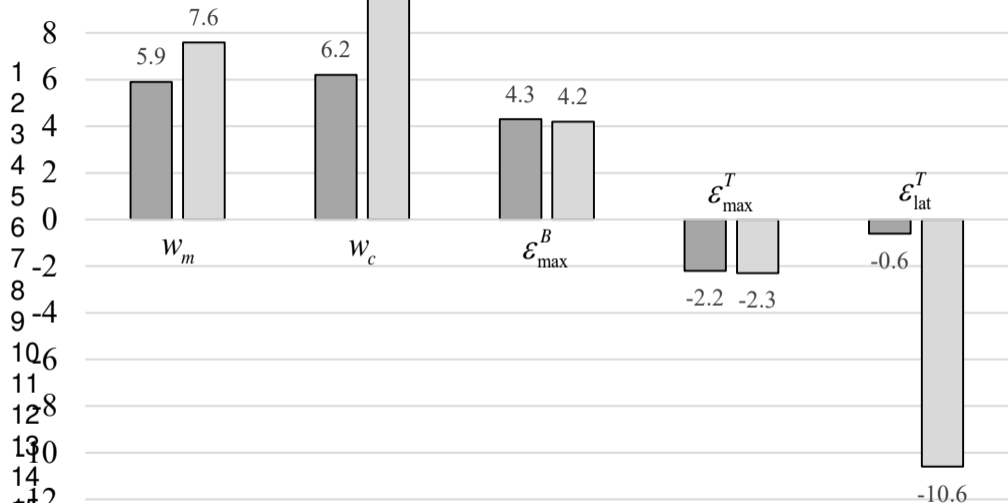
<http://mc.manuscriptcentral.com/jssm>

■ RZT □ TBT ($k^2 = 2.91 \times 10^{-3}$)



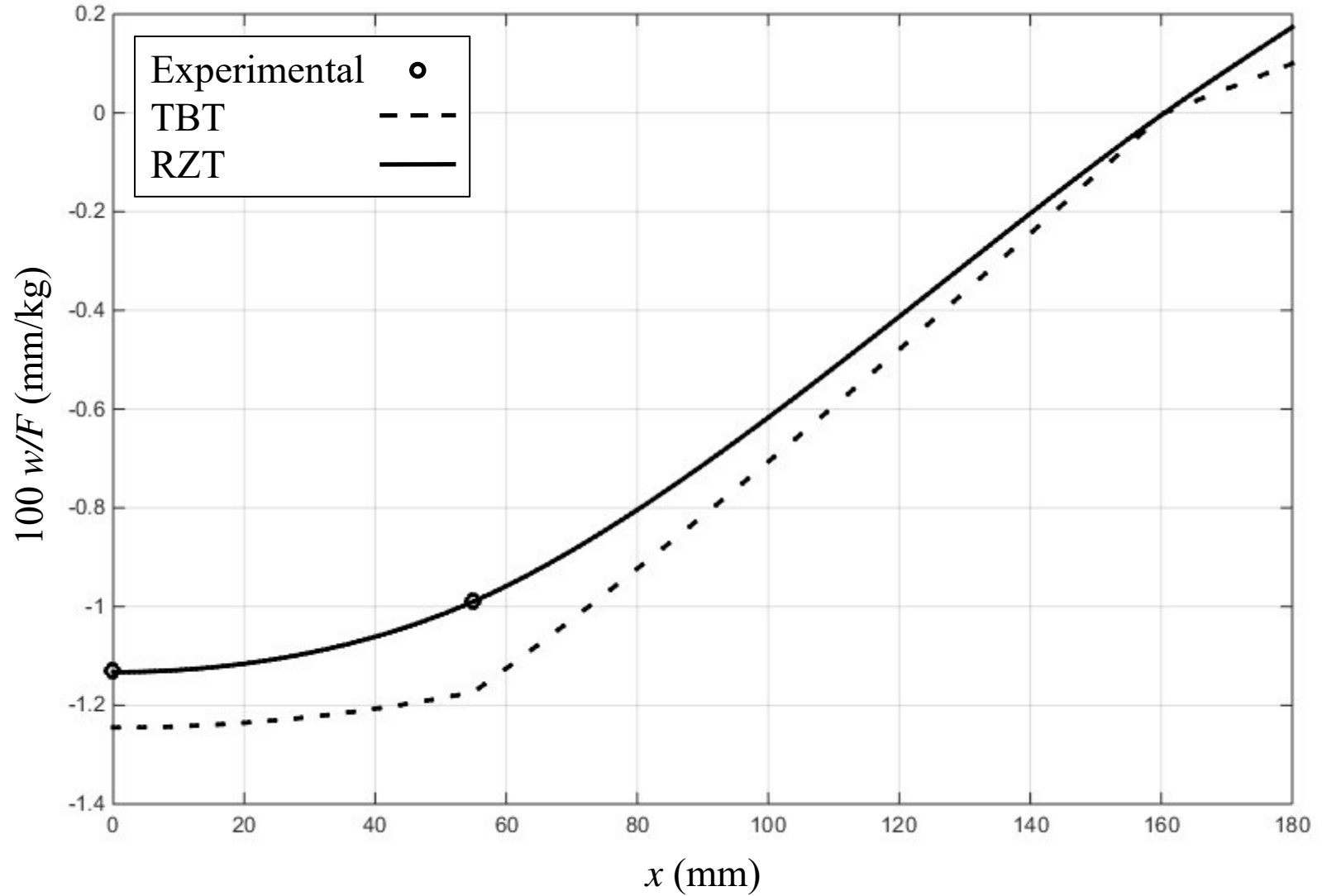
<http://mc.manuscriptcentral.com/jssm>

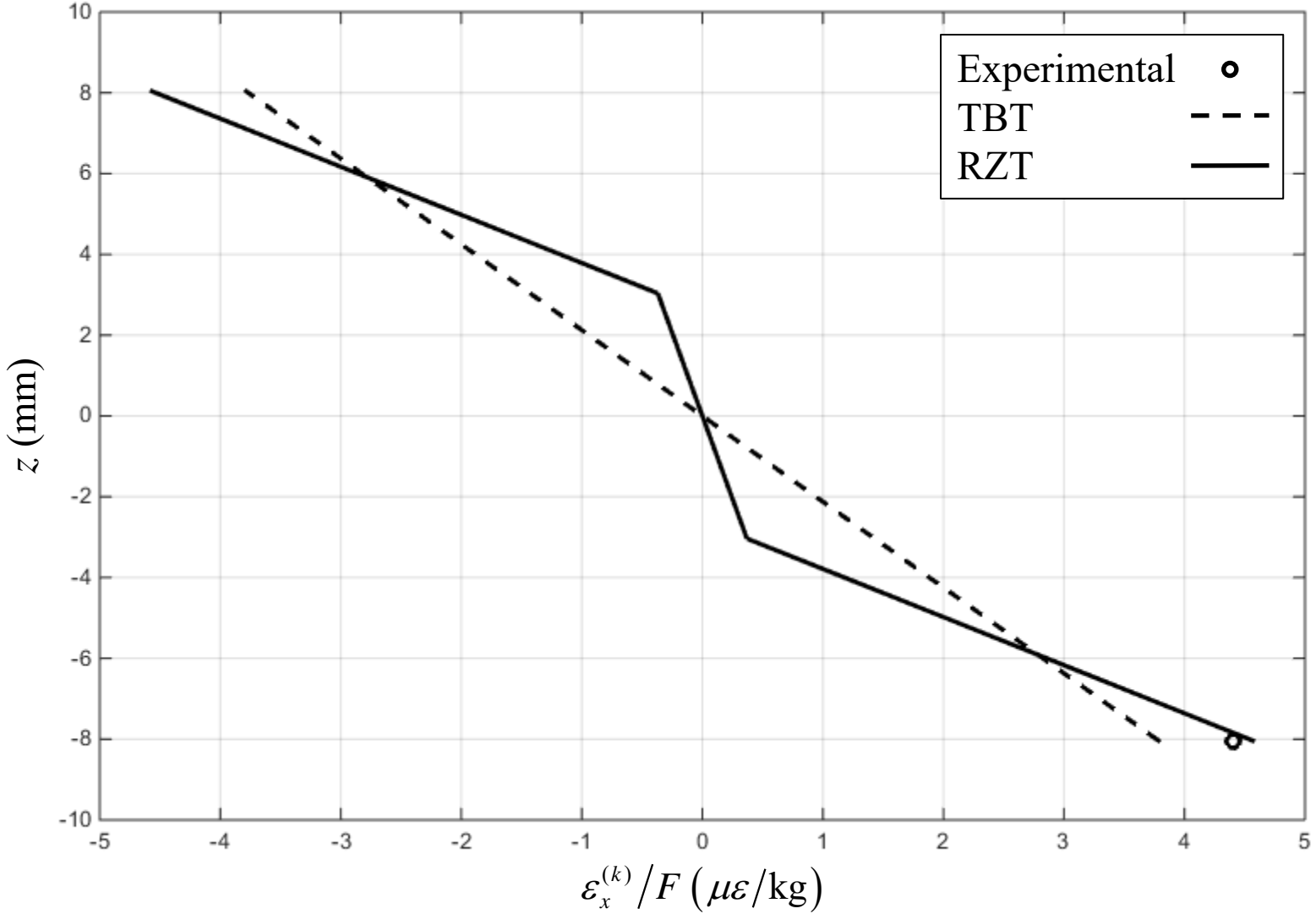
■ RZT □ TBT ($k^2=1.53e-2$)



<http://mc.manuscriptcentral.com/jssm>

■ RZT □ TBT ($k^2=4.95e-3$)





1
2
3
4
5
6
7
8
9
10
11
12
13
14
15
16
17
18
19
20
21
22
23
24
25
26
27
28
29
30
31
32
33
34
35
36
37
38
39
40
41
42
43

